Inorganic Chemistry

pubs.acs.org/IC Article

Visible-Light-Driven C−N Bond Formation by a Hexanickel Cluster Substituted Polyoxometalate-Based Photocatalyst

Jie Li, Jiachen jiao, Jiangnan Chang, Mingxue Li,* and Qiuxia Han*

Cite This: *Inorg. Chem.* 2021, 60, 10022−10029 Read Online

ABSTRACT: A powerful and attractive route to develop novel photocatalysts for C−N bond formation involves the use of pyrrolidine as the substrate and cocatalyst simultaneously. Herein, a new polyoxometalate (POM)-based metal−organic framework, namely, $[Ni_6(OH)_3(H_2O)_9(DPNDIH)(SiW_9O_{34})]_2\cdot 2H_2O$ (SiW_9Ni_6-DPNDI) (DPNDI = *N*,*N*′-di(4-pyridyl)-1,4,5,8-naphthalenediimide), was prepared by incorporating a Ni_6 cluster-substituted POM anion and a photosensitizer (DPNDI) into a framework. The anion···π interactions and covalent bonds between SiW_9Ni_6 and DPNDI are beneficial for the consecutive electron separation and transfer. Under visible-light irradiation, DPNDI can be easily excited to generate radical species DPNDI* that could be further excited in the presence of the electron donor pyrrolidine for the inert O_2 activation. SiW_9Ni_6-DPNDI showed a high efficiency in the photocatalysis of C−N bond formation under a mild condition by the synergy of DPNDI and SiW_9Ni_6. The results of the reaction were confirmed by gas chromatography and ^{1}H NMR. In addition, SiW_9Ni_6-DPNDI exhibited a high sustainability without an obvious change in yields after five cycles.

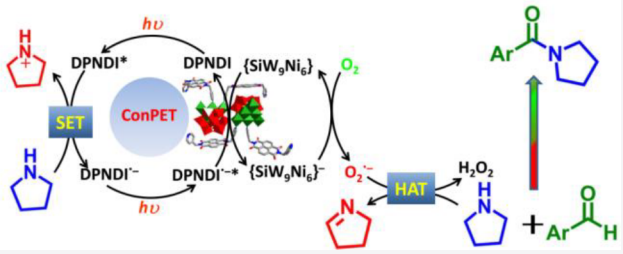

INTRODUCTION

A conventional self-catalysis (SA) converts substrates into products by the generated product catalysts. They have been developed in biological processes and many organic reactions.[1] Comparatively, it will be an effective approach to develop a new SA in which the substrates as the cocatalyst assist the completion of the catalytic cycle. Pyrrolidine is an important substrate for the C−N bond formation. More importantly, it is a star small-molecule catalyst, which has been well-applied in the reactivation of carbonyl compounds by an enamine and imine mechanism.[2,3] Pyrrolidine not only can act as an electron donor but also can participate in the redox by a hydrogen atom transfer (HAT) process. It will be a good choice to develop new photocatalysts for the C−N bond formation with pyrrolidine as a substrate and cocatalyst simultaneously.

The C−N bond formation in organic synthesis has figured prominently due to the indispensable and ubiquitous presence of it in agrochemical, pharmaceutical, and material science.[4] As such, the palladium-catalyzed Buchwald-Hartwig reaction, the Cu-mediated Ulmann reaction, and the Chan-Lam coupling for the C−N bond cross-coupling had served as powerful approaches.[5−7] Despite their versatility, the reactions usually rely on high temperature, rigorous anhydrous and anaerobic manipulation, and high cost. In consideration of this, researchers have tried to utilize nickel-based catalysts to replace them since they are inexpensive and have comparable features, especially for the C−N bond formation.[8,9] Much effort has been made in the past years to push the catalytic efficiency of nickel.[10,11] The Ni-based catalysts for the C−N bond cross-coupling reaction showed a higher activity than the reported catalysts, such as Pd, Cu, and others.[12]

In recent years, visible-light-mediated organic synthesis has emerged as an economical and significant solution in this area.[13−15] Predominately, a photoredox system of dual catalysts, a Ni catalyst along with a photocatalyst, for the C−N bond formation has been proposed, such as $[Ir(dF(CF_3)\text{-}ppy)_2(dtbbpy)]PF_6$ and $[Ru(bpy)_3]Cl_2$ (ppy = polypyrrole; bpy = 2,2′-bipyridine; dtbbpy = di-*tert*-butyl bipyridine).[16] However, these expensive photocatalysts possess a severe limitation due to their sustainability and scalability. By contrast, polyoxometalates (POMs), as the metal−oxygen cluster, have attracted considerable attention due to their controllable structure and significant photochemical activity, for example, reversible multielectron redox transformation properties.[17,18] POMs could be easily reduced to form heteropoly blues under light irradiation.[19] In 2015, silicotungstic acid was successfully utilized as a photocatalyst for the C−N bond formation under a mild condition.[20] Especially, transition-metal cluster-substituted POMs (TMSPs) not only

Received: April 29, 2021
Published: June 16, 2021

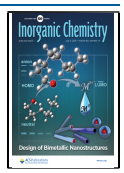

https://doi.org/10.1021/acs.inorgchem.1c01311
Inorg. Chem. 2021, 60, 10022−10029

can modulate the oxidation−reduction potential but also can regulate the photocatalytic performance.[21,22]

Metal−Organic frameworks (MOFs) are a class of porous materials that have a large pore volume, an adjustable shape, and a high amount of surface area. MOFs have shown potential for applications in photocatalysis via a modulation of metal nodes and organic ligands.[23−25] The immobilization of TMSPs into MOFs by a coordination with organic ligands and metal nodes not only can retain and enhance the individual functionalities but also can synergistically provide new features that are different from either building block.[26] *N*,*N*′-Bis(4-pyridylmethyl)naphthalenediimide (DPNDI), in which a π-aromatic system could generate a conspicuous change in the photophysical feature by $\pi\cdots\pi$ interactions of the NDI units, has attracted great attention in chromophoric materials.[27] Under visible-light irradiation, DPNDI can be easily excited to generate the radical species DPNDI* and a photoelectron. In addition, DPNDI can form DPNDI·$^-$ in the presence of an electron donor under a consecutive light irradiation. DPNDI·$^-$ could be further excited to generate DPNDI·$^-$*.[28] It has been widely used to reduce aryl halides, oxidate toluene, and couple amines.[29−31] The development of a novel photocatalyst that incorporates an electron donor and acceptor, using pyrrolidine as a substrate and cocatalyst, will contribute to the consecutive photoinduced electron transfer (ConPET) for the C−N bond formation.

Considering above aspects, a new Ni_6 cluster-substituted POM-incorporated MOF (POMOF) $[Ni_6(OH)_3(H_2O)_9(DPNDIH)(SiW_9O_{34})]_2\cdot 2H_2O$ (SiW_9Ni_6-DPNDI) was prepared by the incorporation of a POM anion, active nickel(II), and photosensitizer DPNDI into one molecule. The combination of TMSP and photosensitizer organic ligand into one framework will improve the interactions between substrates and catalyst to facilitate a heterogeneous photocatalysis. In the structure, the anion$\cdots\pi$ interactions and coordination bonds between SiW_9Ni_6 and DPNDI are beneficial for the electron separation and transfer. Under consecutive light irradiation, DPNDI will be excited to generate DPNDI·$^-$* in the presence of pyrrolidine and photoelectron, which can transfer to the electron acceptor of SiW_9Ni_6 through single electron transfer (SET) process, after which, POM anion will active O_2 to generate $O_2\cdot^-$ (Scheme 1), which could absorb the H atom of the substrate to generate H_2O_2 that is beneficial for the oxidative amidation of an aryl aldehyde. Thus, the synergy of DPNDI and SiW_9Ni_6 will be conductive to the photocatalysis of the C−N bond formation under a mild condition by the ConPET process.

Scheme 1. Design Concept of SiW_9Ni_6-DPNDI for the Photocatalysis of the C−N Bond Formation

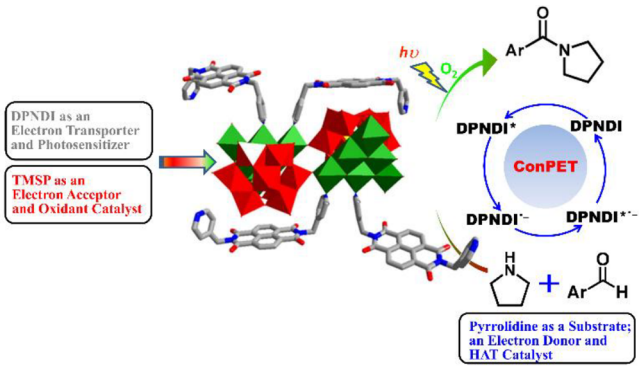

RESULTS AND DISCUSSION

Single-crystal X-ray diffraction revealed that SiW_9Ni_6-DPNDI crystallizes in the monoclinic space group *C*2/*c*. The asymmetric unit of SiW_9Ni_6-DPNDI consists of one Ni_6-substituted trivacant Keggin-type POM $\{SiW_9Ni_6\}$, one DPNDI ligand, and one water molecule. A bond valence sum (BVS) calculation and X-ray photoelectron spectroscopy (XPS) tests indicated that all the atoms of Si, W, and Ni were +4, +6, and +2 oxidation states, respectively. Four oxygen atoms of O35, O36, O37, and O43 were monoprotonated (Table S2). In the $\{Ni_6\}$ fragments, all of the Ni atoms are six-coordinated with a distorted octahedron geometry (Figure S1). Each Ni(II) ion is coordinated with water. The lability of the coordinated water molecules allows SiW_9Ni_6-DPNDI to act as Lewis acid catalytic sites for activating the substrate of benzaldehyde. In the structural unit of SiW_9Ni_6-DPNDI, two $\{SiW_9Ni_6\}$ fragments are linked together by two Ni−O−W bonds to form a dimer with the angle of 140.874(5)°. Afterward, the dimer as a secondary building unit coordinates with four N atoms of four DPNDI ligands (Figure 1). Figure 2a shows the ellipsoidal plot of the structural unit of SiW_9Ni_6-DPNDI. Two neighboring SiW_9Ni_6-DPNDI units were linked to each other by Ni−N bonds to form a two-dimensional (2D)

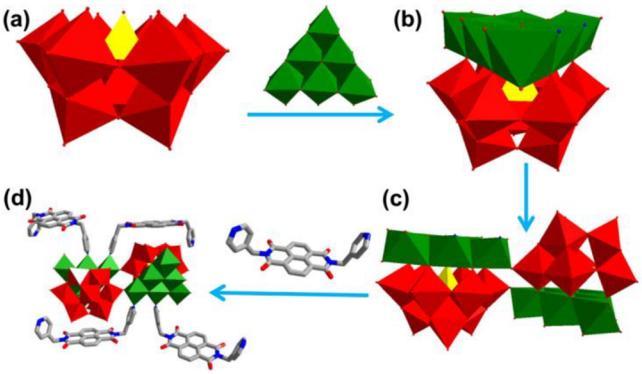

Figure 1. Schematic view of the structural unit of SiW_9Ni_6-DPNDI.

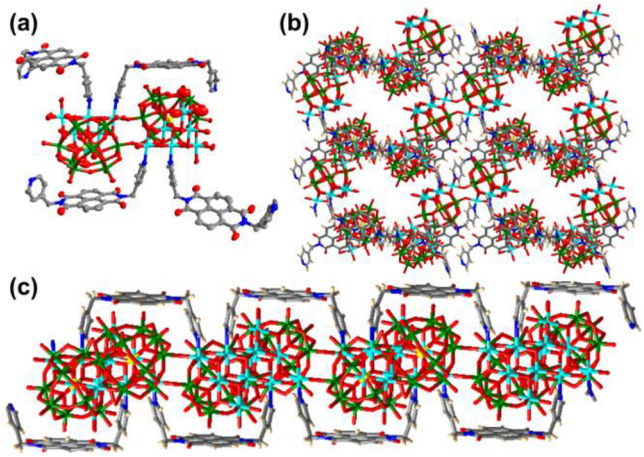

Figure 2. (a) Ellipsoid model of SiW_9Ni_6-DPNDI. (b) Representation of the 2D network along the *a*-axis. (c) View of the 1D chain along the *b*-axis.

https://doi.org/10.1021/acs.inorgchem.1c01311
Inorg. Chem. 2021, 60, 10022−10029

structure along the *a*-axis, which can be seen as a network structure (Figure 2b). Along the *b*-axis, the structure is a one-dimensional (1D) chain (Figure 2c). The size of the hole is 18.14 Å × 8.43 Å (atom-to-atom distance). The 2D structure further stacked to form a three-dimensional (3D) network structure by a $\pi\cdots\pi$ interaction effect. The accessible pores are ~6883.6 $Å^3$ (39.3%) calculated from a PLATON analysis, suggesting the possibility to absorb suitable substrates within the channels of the SiW_9Ni_6-DPNDI.[32] In the structure, the anion$\cdots\pi$ interactions and coordination bonds between SiW_9Ni_6 and DPNDI are beneficial to the electron separation and transfer. Note that the POMOF containing SiW_9Ni_6 units had remained unexplored at the present time.

The phase purity of SiW_9Ni_6-DPNDI was confirmed by powder X-ray diffraction (PXRD) patterns (Figure S2). The Fourier transform infrared (FTIR) spectra of SiW_9Ni_6-DPNDI and DPNDI are shown in Figure S3. For the comparison of two spectra, the characteristic peak of DPNDI of SiW_9Ni_6-DPNDI shows a slightly blue shift due to the interaction between metal ions and DPNDI. Both spectra display strong peaks from 1700 to 1580 cm^{-1}. They correspond to C═O, N−H, and C−H bond stretching vibrations of the DPNDI ligand, and the peaks between 1450 and 1175 cm^{-1} are ascribed to the C−N bond stretching vibrations of the DPNDI ligand.[33] In the spectrum of SiW_9Ni_6-DPNDI, the strong peak at 3423 cm^{-1} corresponds to the bending vibration mode of H_2O. The peaks at 1041 and 941 cm^{-1} correspond to Si−O and W−O_t stretching vibrations. The peaks at ~881, 776, and 700 cm^{-1} are ascribed to the W−O_b−W stretching vibration.[34] The thermogravimetric analysis (TGA) curve of SiW_9Ni_6-DPNDI is shown in Figure S4. The weight loss in the temperature range of 30−1000 °C corresponds to the removal of 2 lattice water molecules, 8 protons, and 18 coordinate water molecules (observed, 7.73%; calcd, 7.25%). The remaining stage in the range of 400−920 °C might be attributed to the loss of four DPNDI ligands and POM anion skeleton decomposition.[35] This result indicates the high thermal stability of SiW_9Ni_6-DPNDI, which plays an important role in heterogeneous catalysis. Figure 3 gives the morphology

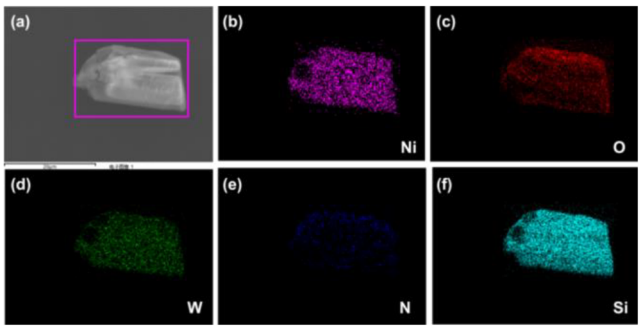

Figure 3. Morphology images of a single crystal of SiW_9Ni_6-DPNDI. (a) Scanning electron microscopy image. (b−g) Elemental mappings of Ni, O, W, N, and Si, respectively.

images of a single crystal of SiW_9Ni_6-DPNDI, which shows a blocky structure. The corresponding element mapping indicates the uniform distribution of Ni, O, W, N, and Si of SiW_9Ni_6-DPNDI. These results further confirm the composition of SiW_9Ni_6-DPNDI.

The elemental composition of SiW_9Ni_6-DPNDI and oxidation states of constituent elements along with binding energy were further analyzed by XPS. The full spectrum of SiW_9Ni_6-DPNDI shows the presence of C, O, N, Si, W, and Ni elements (Figure 4a). The deconvolution of the C 1s spectrum into four peaks of binding energy 288.1, 285.6, 284.9, and 284.3 eV correspond to the C═O, C−N, C−C, and C−H bonds, respectively[36] (Figure 4b). Meanwhile, the two peaks of nitrogen spectra at 400.4 and 399.6 eV represent the C−N bond of DPNDI. The other peak at 398.9 eV represents the Ni−N bond[37] (Figure 4c). The signal of Si 2p exhibits one peak for Si^{4+} at binding energy 101.7 eV (Figure 4d). The W 4f signal exhibits two peaks at 37.5 eV ($4f_{5/2}$) and 35.4 eV ($4f_{7/2}$) that are assigned to the W^{6+} environment[38] (Figure 4e). The peaks centered at 873.3 and 885.5 eV are ascribed to the bivalent state Ni^{2+} $2p_{1/2}$ and Ni^{2+} $2p_{3/2}$ with two satellite peaks located at 879.8 and 861.6 eV, respectively[39] (Figure 4f).

SiW_9Ni_6-DPNDI contains a Ni_6 cluster, which shows a ferromagnetic exchange interaction. This has been explored in similar structures.[40−42] Therefore, the ferromagnetic exchange interaction might exist in the SiW_9Ni_6-DPNDI. In order to verify this speculation, the magnetic property of SiW_9Ni_6-DPNDI was preliminary explored. The field-dependent magnetization curve $M(H)$ of SiW_9Ni_6-DPNDI at 2 K represented a continuous increase (Figure 5a). The value of 29.39 Nβ at ca. 70 kOe tends to reach the saturation state. The magnetic susceptibility (χ_m) of SiW_9Ni_6-DPNDI was also measured from 1.8 to 300 K under an external magnetic field of 1000 Oe. The plots of χ_m versus T and $\chi_m T$ versus T are shown in Figure 5b. At 300 K, the χ_m value of SiW_9Ni_6-DPNDI was 0.0852 emu mol^{-1}. When cooled, the χ_m value slowly increased to 0.6509 emu mol^{-1} at 50 K. Afterward, the χ_m value quickly reached a maximum of 6.606 emu mol^{-1} at 1.8 K. The $\chi_m T$ value of SiW_9Ni_6-DPNDI was 25.56 emu mol^{-1} K at 300 K; thereafter, the value gradually increased to a maximum of 40.14 emu mol^{-1} K at 16 K. Then, the value decreased sharply to 11.89 emu mol^{-1} K at 1.8 K. The sudden decrease might be because of the presence of the zero-field splitting effect.[43] Moreover, the plot of $1/\chi_m$ versus T obeyed the Curie−Weiss equation at the temperature of 1.8−300 K with a positive Curie constant C = 24.44 cm^3 K mol^{-1} and Weiss constant θ = 3.637 K (Figure S6). These results indicated the ferromagnetic coupling between the Ni^{2+} ions of SiW_9Ni_6-DPNDI.

The UV−vis spectrum of SiW_9Ni_6-DPNDI exhibited broad and strong absorption peaks between 200 and 800 nm, which indicated its potential application in photocatalysis (Figure 6a). The absorption peaks at 365, 390, and 411 nm correspond to the DPNDI ligand. The absorption peak at 680 nm corresponds to the charge transfer of DPNDI to POMs.[44] With the white light-emitting diode (LED) irradiation of 20 min, the absorbance peak intensity increased. After pyrrolidine was added and the sample was irradiated for another 10 min, the peaks at ~504, 680, and 765 nm increased clearly, and a new peak at ~610 nm appeared. That corresponded to the generation of DPNDI* and POM_{red}.[28] Meanwhile, the fluorescence of SiW_9Ni_6-DPNDI changed dramatically (Figure 6c), which should be attributed to the electron transfer from the excited DPNDI ligand. Figure 6d indicated that the emission intensities of SiW_9Ni_6-DPNDI also decreased with the addition of pyrrolidine amounts. Therefore, there might have been a sequential electron transfer process between the SiW_9Ni_6-DPNDI and pyrrolidine during the irradiation. According to a Tauc plot, the bond-gap value estimated of SiW_9Ni_6-DPNDI was 2.79 eV (Figure S7). To verify the

https://doi.org/10.1021/acs.inorgchem.1c01311
Inorg. Chem. 2021, 60, 10022−10029

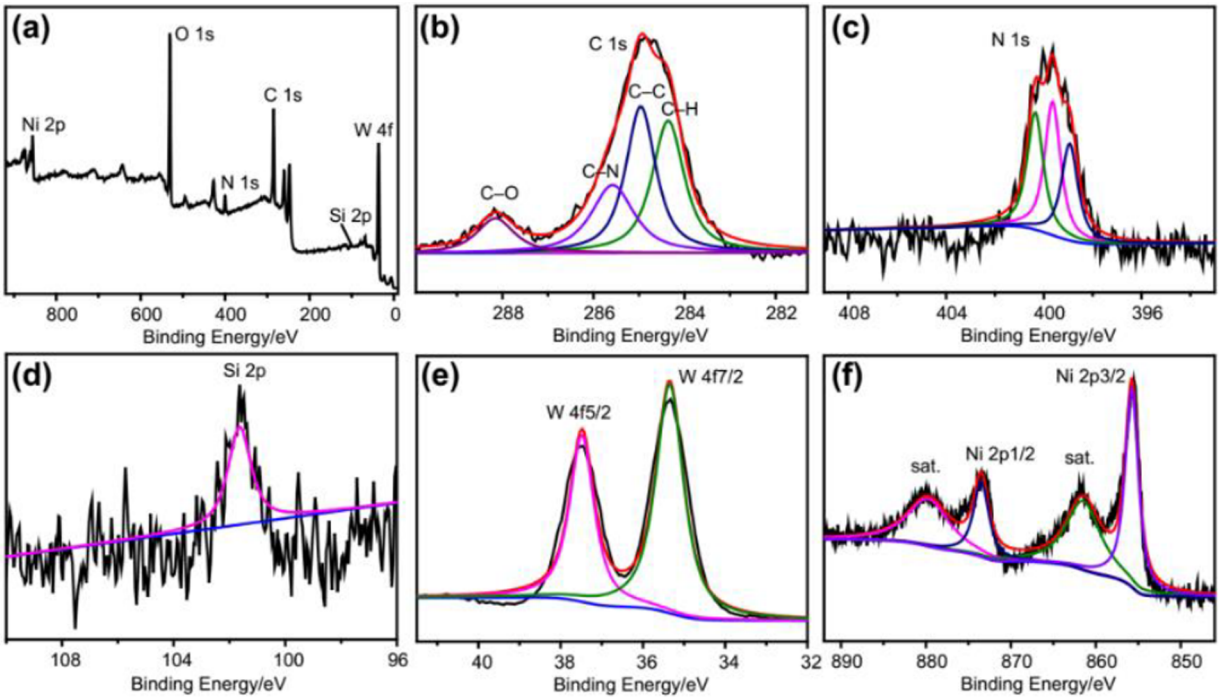

Figure 4. XPS spectra of (a) SiW_9Ni_6-DPNDI, (b) C 1s, (c) N 1s, (d) Si 2p, (e) W 4f, and (f) Ni 2p.

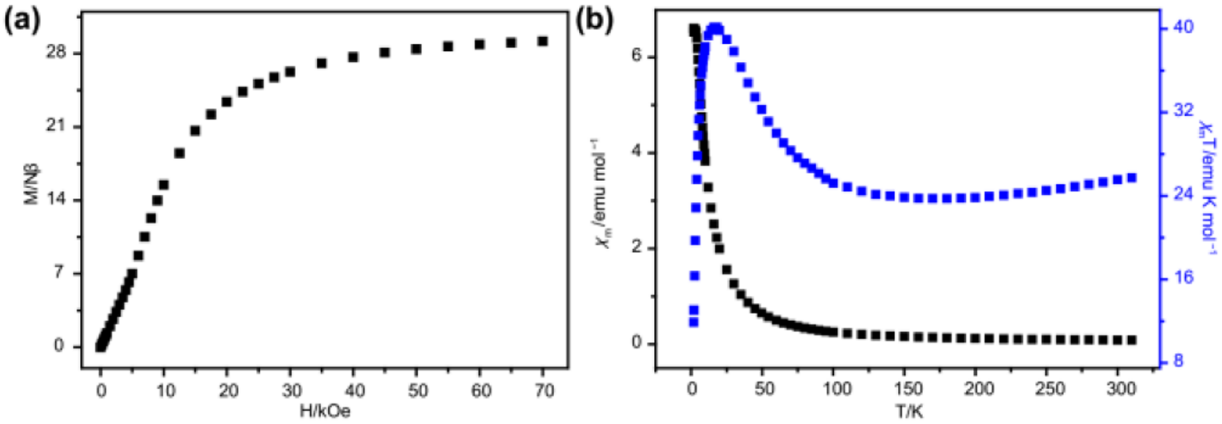

Figure 5. (a) The field-dependent magnetization curve $M(H)$ of SiW_9Ni_6-DPNDI. (b) Temperature dependence of χ_m and $\chi_m T$.

semiconductor property of SiW_9Ni_6-DPNDI and the possibility of a photocatalyzed C−N bond formation, Mott−Schottky tests at frequencies of 3000, 3500, and 4000 Hz were performed (Figure 6b). The results indicated that SiW_9Ni_6-DPNDI was a typical n-type semiconductor. Considering that the frequency was independent of the interaction point, the position of SiW_9Ni_6-DPNDI was estimated to be −1.40 V. Thus, the bottom of the conduction band (lowest unoccupied molecular orbital (LUMO)) of SiW_9Ni_6-DPNDI was estimated to be −1.20 V versus the normal hydrogen electrode (NHE). The valence band (highest occupied molecular orbital (HOMO)) position of SiW_9Ni_6-DPNDI was calculated to 1.57 V versus NHE. Meanwhile, the TMSP SiW_9Ni_6, as a reference, was also explored (Figures S8−S10). The values of LUMO and HOMO positions of SiW_9Ni_6 were estimated to be −0.92 and 1.67 V versus NHE, respectively. Because their LUMO positions are more negative than $E(O_2/O_2{\cdot}^-) = -0.33$ V,[45] it was feasible theoretically to use SiW_9Ni_6-DPNDI or SiW_9Ni_6 as a photocatalyst for the reduction of O_2 to $O_2{\cdot}^-$. That can absorb the H atom of pyrrolidine to generate H_2O_2, which is beneficial for the oxidative amidation of aryl aldehyde.[46,47]

The coupling of pyrrolidine with *p*-chlorobenzaldehyde was taken as a model reaction. Under the optimum reaction condition, the product (4-chlorophenyl)(pyrrolidin-1-yl)-methanone was obtained in 88% yield (Table 1, Entry 1). Control experiments indicated the importance of catalyst SiW_9Ni_6-DPNDI, light, K_2CO_3, and O_2 for the C−N bond formation (Table 1, Entries 2−5). Upon the addition of 0.1 mol *p*-benzoquinone (BQ), as a superoxide anion scavenger, the yield of the reaction was greatly decreased to 8% (Table 1, Entry 6). Under the same condition, without the DPNDI ligand or SiW_9Ni_6, the yields (40% and 80%) were lower than those of the SiW_9Ni_6-DPNDI that contains both in a structure (Table 1, Entries 7 and 8). Thus, the DPNDI and SiW_9Ni_6 might give a catalytic synergy for the C−N bond coupling in the framework of SiW_9Ni_6-DPNDI. The SiW_9Ni_6-DPNDI catalyst was tested and recycled through at least five cycles without any significant degradation of activity (Figure 7). The

https://doi.org/10.1021/acs.inorgchem.1c01311
Inorg. Chem. 2021, 60, 10022−10029

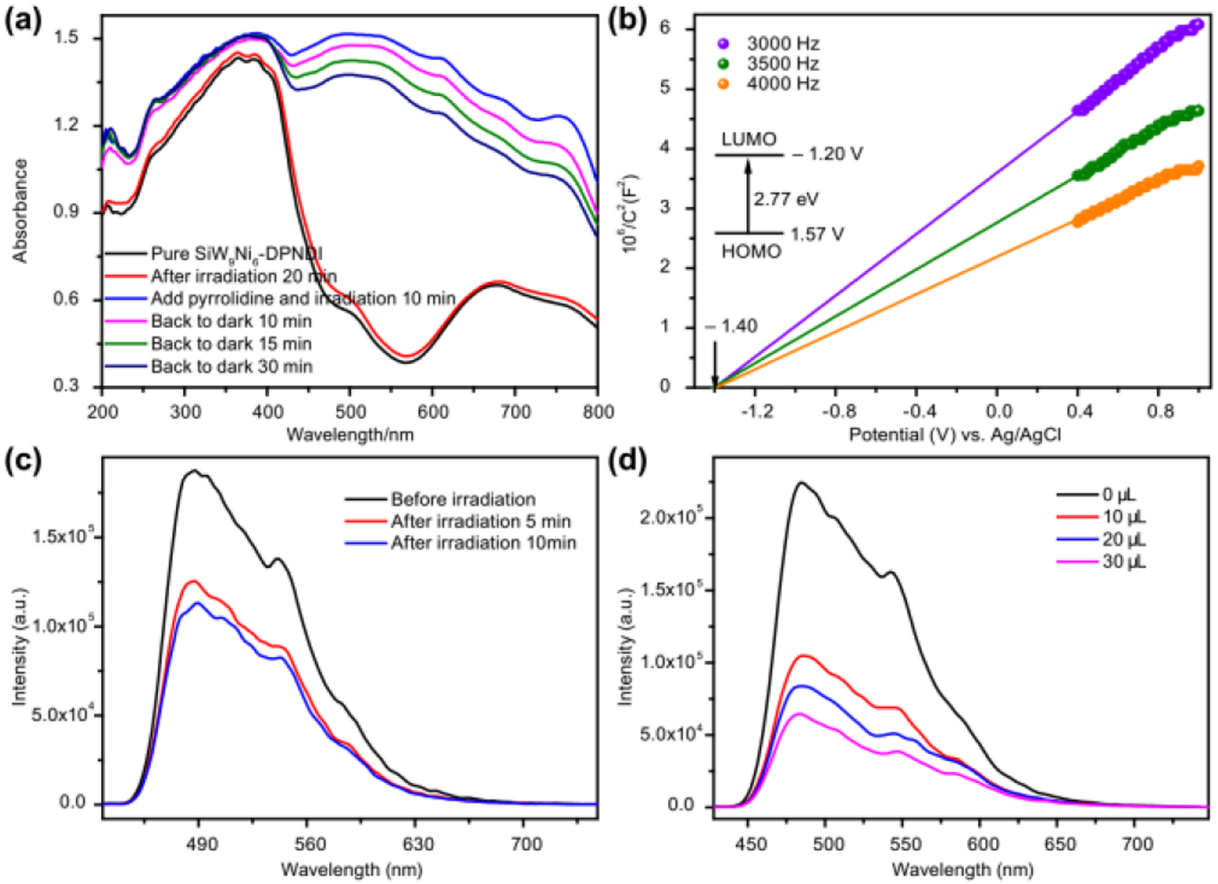

Figure 6. (a) The formation of DPNDI* and POM_{red} under light irradiation. (b) Mott–Schottky plots of SiW_9Ni_6-DPNDI. (c) Photoluminescence and (d) the addition of pyrrolidine fluorescence spectra (Ex = 424 nm) of SiW_9Ni_6-DPNDI upon visible-light irradiation.

Table 1. Control Experiments for the Photoredox C–N Bond Formation[a]

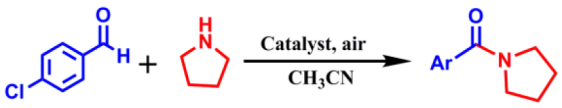

entry	catalysts	yield[b] (%)
1	SiW_9Ni_6-DPNDI	88
2[c]	SiW_9Ni_6-DPNDI	
3		
4[d]	SiW_9Ni_6-DPNDI	59
5[e]	SiW_9Ni_6-DPNDI	8
6[f]	SiW_9Ni_6-DPNDI	8
7	$\{SiW_9Ni_6\}$	40
8	DPNDI	80

[a]Reaction condition: catalyst, 2 μmol; aryl aldehyde 0.025 mmol; K_2CO_3 0.07 mmol; pyrrolidine 0.75 mmol; CH_3CN, 1 mL; 10 W white LED lamp; temperature, 25 ± 5 °C; 24 h; in the air. [b]Yields were confirmed by GC. [c]Without light. [d]Without K_2CO_3. [e]BQ as superoxide anion scavenger. [f]N_2 atmosphere.

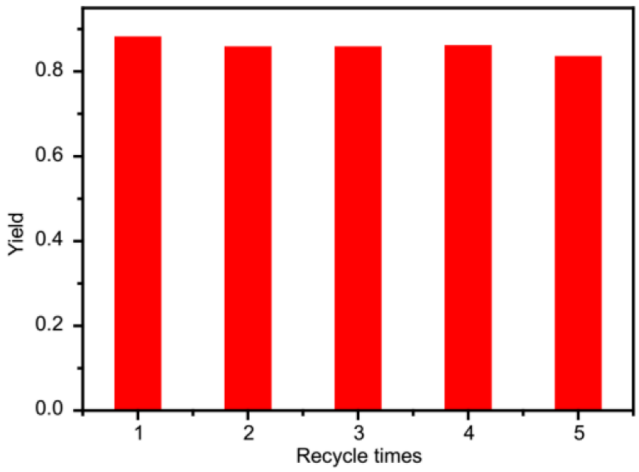

Figure 7. Five cycles of the photocatalytic C–N bond formation.

good durability was confirmed by FTIR and PXRD spectra (Figure S11).

Under the optimum conditions, the scope of the aromatic aldehydes for the C–N band formation was expanded (Table 2). All of the products were confirmed by ^{1}H NMR. The aromatic-bearing electron-donating substituents of *p*-CH_3 and *p*-OCH_3 gave a lower yield (38% and 35%) than electron-withdrawing substitutes of *p*-Br and *p*-NO_2 (86% and 90%). The electron-withdrawing group at the *meta* position of (2-nitrophenyl)(pyrrolidin-1-yl)methanone gave a yield of 49% due to steric hindrance. In addition, the aromatic aldehyde derivatives of 2-naphthaldehyde and 4-pyridinecarboxaldehyde were also feasible. The corresponding yields were 70% and 76%, respectively. Meanwhile, the substrate scope of pyrrolidine was also expanded to other amines reacting with 4-nitrobenzaldehyde, such as morpholine, hexamethylenimine, 1-methylpiperazine, and 1,2,3,4-tetrahydroisoquinoline. The

https://doi.org/10.1021/acs.inorgchem.1c01311
Inorg. Chem. 2021, 60, 10022–10029

Table 2. Scope of the Photocatalytic Reaction for Aldehydes and Amines under the Optimum Condition

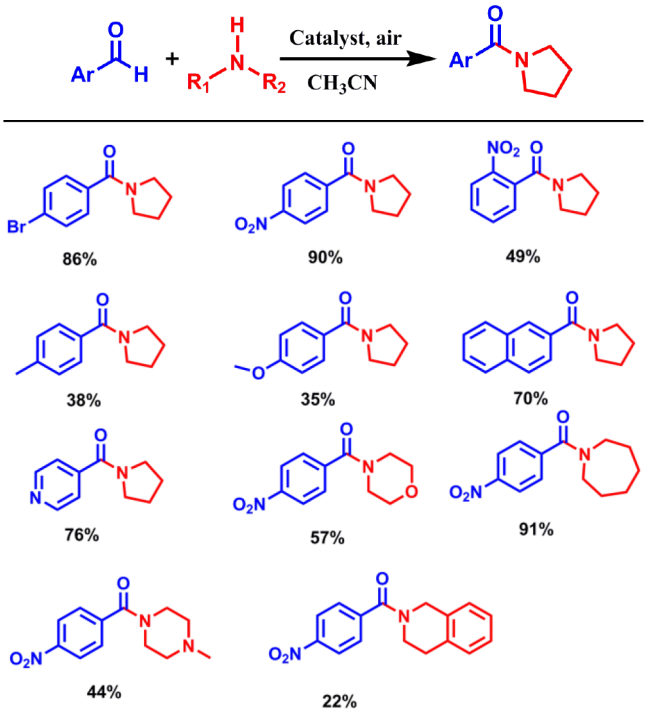

corresponding yields were 57%, 91%, 44%, and 22%, respectively.

On the basis of these studies, a plausible mechanism was proposed (Scheme 2). Under visible-light irradiation with

Scheme 2. Proposed Catalytic Mechanism of C−N Bond Formation over SiW_9Ni_6-DPNDI

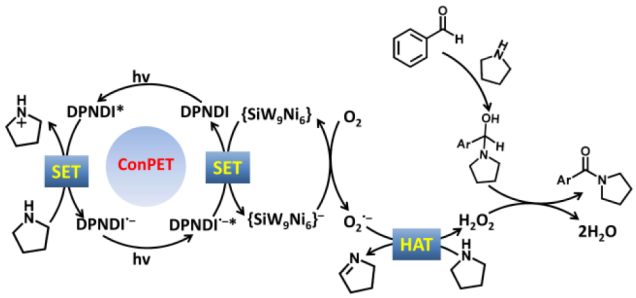

SiW_9Ni_6-DPNDI, the DPNDI of the structure gave an excited DPNDI* species, after which pyrrolidine as a cocatalyst gave an electron to it to generate DPNDI·$^-$. A continuous irradiation of DPNDI·$^-$ with visible light gave a DPNDI·$^{-*}$ and a photoelectron, which through an SET process to the TMSP $\{SiW_9Ni_6\}$ changed it to $\{SiW_9Ni_6\}^-$. Meanwhile, with the reoxidation of $\{SiW_9Ni_6\}^-$, O_2 was reduced to the superoxide radical $O_2\cdot^-$, which absorbed the H atom of pyrrolidine to generate H_2O_2. The intermediate was confirmed by ^{1}H NMR (Figure S12). The nucleophilic attack of pyrrolidine with aldehyde gave the intermediate of acetal or aminal adduct, which was oxidized by H_2O_2 to generate the desired product.[48]

CONCLUSIONS

In summary, a new TMSP-based POMOF SiW_9Ni_6-DPNDI for the photocatalysis of a C−N bond formation was prepared and characterized systematically under a mild condition. The terminal oxygen atoms, nitrogen atoms, counter cations H^+, and water molecules of the structure give a high proton conductivity of 1.18×10^{-4} S cm^{-1} at 358 K and 98% relative humidity. The magnetic property tests showed that SiW_9Ni_6-DPNDI gave a ferromagnetic coupling between the Ni(II) ions. Moreover, SiW_9Ni_6-DPNDI exhibited a good efficiency of coupling amines and aromatic aldehydes under visible-light irradiation. The synergy between SiW_9Ni_6 and the DPNDI ligand offered a simple, green, and sustainable method for the C−N bond formation. In the reaction, pyrrolidine not only was used as an important substrate but also acted as a cocatalyst of an electron donor participant in the redox. Our ongoing efforts strive to construct novel functional POMOFs that are involved in the photocatalytic organic synthesis of valued compounds.

EXPERIMENTAL SECTION

Preparations of $[Ni_6(OH)_3(H_2O)_9(DPNDIH)(SiW_9O_{34})]_2\cdot 2H_2O$ (SiW_9Ni_6-DPNDI). SiW_9Ni_6-DPNDI was prepared by a hydrothermal method. $Na_{10}[\alpha\text{-}SiW_9O_{34}]\cdot 18H_2O$ (0.2 g, 0.07 mmol), DPNDI (0.015 g, 0.03 mmol), and $NiSO_4\cdot 6H_2O$ (0.1 g, 0.4 mmol) were added to a CH_3CN/H_2O (8 mL, v/v = 1:3) binary solution and stirred for 12 h, and the pH was adjusted to 4.84 with 3 mol L^{-1} HCl. The obtained solution was sealed in a 25 mL Teflon-lined stainless reactor and kept at 120 °C for 4 d. After it cooled to room temperature, yellow-green color crystals of SiW_9Ni_6-DPNDI were obtained (Yield, 19.2%, based on $Na_{10}[\alpha\text{-}SiW_9O_{34}]$). Anal. Calcd for $C_{104}H_{116}N_{16}O_{112}Ni_{12}Si_2W_{18}$ (%): C 9.58, H 1.24, N 1.72, Si 0.86, Ni 10.80, W 50.76. Found: C 9.46, H 1.14, N 1.83, Si 0.81, Ni 10.83, W 50.86.

Photocatalytic C−N Coupling Reaction. The photocatalytic process was taken on a photoreactor (WP-TEC-1020HSL, Wattecs Lab Equiment Co., Ltd.) with continuous cooling water equipment. In a typical reaction system, a 15 mL quartz tube equipped with a stir bar was charged with 2 μmol of photocatalyst SiW_9Ni_6-DPNDI, 0.025 mmol of aryl aldehyde, 0.75 mmol of pyrrolidine, 0.07 mmol of K_2CO_3, and 1 mL of CH_3CN. The resulting mixture was allowed to react in atmospheric conditions. A 10 W white LED lamp was used as the light source by bottom irradiation. The quartz tube was placed ~0.5 cm from the light. The temperature of the reaction was in the range of 25 ± 5 °C. The intensity of the incident light was ca. 320 mW/cm^2, which was tested by a photometer (CEL-NP2000, Beijing China Education Aulight Co., Ltd.). The irradiated surface area of the mixture was ~9.04 cm^2. After 24 h of reaction, the yield was confirmed by a gas chromatography (GC) analysis. The desired product was isolated with a silica gel column using petroleum ther/ethyl acetate (EtOAc) as eluent.

ASSOCIATED CONTENT

Supporting Information

The Supporting Information is available free of charge at https://pubs.acs.org/doi/10.1021/acs.inorgchem.1c01311.

Materials and characterizations, X-ray crystallography, Ni_6 cluster spectrum, FTIR, PXRD, and TGA spectra, proton conductivity, χ_m^{-1} versus T curve, Tauc plot, UV−vis spectra, Mott-Scotty curve, ^{1}H NMR data (PDF)

Accession Codes

CCDC 2053687 contains the supplementary crystallographic data for this paper. These data can be obtained free of charge via www.ccdc.cam.ac.uk/data_request/cif, or by emailing data_request@ccdc.cam.ac.uk, or by contacting The Cam-

https://doi.org/10.1021/acs.inorgchem.1c01311
Inorg. Chem. 2021, 60, 10022−10029

bridge Crystallographic Data Centre, 12 Union Road, Cambridge CB2 1EZ, UK; fax: +44 1223 336033.

■ AUTHOR INFORMATION

Corresponding Authors

Mingxue Li − *Henan Key Laboratory of Polyoxometalates, Institute of Molecular and Crystal Engineering, College of Chemistry and Chemical Engineering, Henan University, Kaifeng 475004, P. R. China;* orcid.org/0000-0003-2760-2020; Email: limingxue@henu.edu.cn

Qiuxia Han − *Henan Key Laboratory of Polyoxometalates, Institute of Molecular and Crystal Engineering, College of Chemistry and Chemical Engineering, Henan University, Kaifeng 475004, P. R. China;* orcid.org/0000-0002-0175-562X; Email: hdhqx@henu.edu.cn

Authors

Jie Li − *Henan Key Laboratory of Polyoxometalates, Institute of Molecular and Crystal Engineering, College of Chemistry and Chemical Engineering, Henan University, Kaifeng 475004, P. R. China; School of Chemistry & Chemical Engineering, Zhoukou Normal University, Zhoukou 466001, P. R. China*

Jiachen jiao − *Henan Key Laboratory of Polyoxometalates, Institute of Molecular and Crystal Engineering, College of Chemistry and Chemical Engineering, Henan University, Kaifeng 475004, P. R. China*

Jiangnan Chang − *Henan Key Laboratory of Polyoxometalates, Institute of Molecular and Crystal Engineering, College of Chemistry and Chemical Engineering, Henan University, Kaifeng 475004, P. R. China*

Complete contact information is available at: https://pubs.acs.org/10.1021/acs.inorgchem.1c01311

Author Contributions

All authors have given approval to the final version of the manuscript.

Notes

The authors declare no competing financial interest.

■ ACKNOWLEDGMENTS

This research was funded by the National Natural Science Foundation of China (21671055, 21601048), Henan University First-class Discipline Cultivation Project (2020YLZDYJ06), the Scientific and Technological Project of Henan province (212102310852), the Key Scientific Research Project of Henan Higher Education Institutions (20ZX006), and the Excellent Youth Foundation of Henan Province (202300410043).

■ REFERENCES

(1) Sawato, T.; Saito, N.; Yamaguchi, M. Chemical Systems Involving Two Competitive Self-Catalytic Reactions. *ACS Omega* **2019**, *4*, 5879−5899.

(2) Le Saux, E.; Ma, D.; Bonilla, P.; Holden, C. M.; Lustosa, D.; Melchiorre, P. A General Organocatalytic System for Enantioselective Radical Conjugate Additions to Enals. *Angew. Chem., Int. Ed.* **2021**, *60*, 2−8.

(3) Mazzarella, D.; Crisenza, G. E. M.; Melchiorre, P. Asymmetric Photocatalytic C−H Functionalization of Toluene and Derivatives. *J. Am. Chem. Soc.* **2018**, *140*, 8439−8443.

(4) Sivaguru, P.; Wang, Z.; Zanoni, G.; Bi, X. Cleavage of Carbon−Carbon Bonds by Radical Reactions. *Chem. Soc. Rev.* **2019**, *48*, 2615−2656.

(5) Sambiagio, C.; Marsden, S. P.; Blacker, A. J.; McGowan, P. C. Copper Catalysed Ullmann Type Chemistry: from Mechanistic Aspects to Modern Development. *Chem. Soc. Rev.* **2014**, *43*, 3525−3550.

(6) Ruiz-Castillo, P.; Buchwald, S. L. Applications of Palladium-Catalyzed C−N Cross-Coupling Reactions. *Chem. Rev.* **2016**, *116*, 12564−12649.

(7) Park, Y.; Kim, Y.; Chang, S. Transition Metal-Catalyzed C−H Amination: Scope, Mechanism, and Applications. *Chem. Rev.* **2017**, *117*, 9247−9301.

(8) Marín, M.; Rama, R. J.; Nicasio, M. C. Ni-Catalyzed Amination Reactions: an Overview. *Chem. Rec.* **2016**, *16*, 1819−1832.

(9) Ananikov, V. P. Nickel: The "Spirited Horse" of Transition Metal Catalysis. *ACS Catal.* **2015**, *5*, 1964−1971.

(10) Corcoran, E. B.; McMullen, J. P.; Lévesque, F.; Wismer, M. K.; Naber, J. R. Photon Equivalents as a Parameter for Scaling Photoredox Reactions in Flow: Translation of Photocatalytic C−N Cross-Coupling from Lab Scale to Multikilogram Scale. *Angew. Chem., Int. Ed.* **2020**, *59*, 11964−11968.

(11) Corcoran, E. B.; Pirnot, M. T.; Lin, S.; Dreher, S. D.; DiRocco, D. A.; Davies, I. W.; Buchwald, S. L.; MacMillan, D. W. C. Aryl Amination Using Ligand-Free Ni(II) Salts and Photoredox Catalysis. *Science* **2016**, *353*, 279−283.

(12) Tassone, J. P.; MacQueen, P. M.; Lavoie, C. M.; Ferguson, M. J.; McDonald, R.; Stradiotto, M. Nickel-Catalyzed N-Arylation of Cyclopropylamine and Related Ammonium Salts with (Hetero)aryl (Pseudo)halides at Room Temperature. *ACS Catal.* **2017**, *7*, 6048−6059.

(13) Schultz, D. M.; Yoon, T. P. Solar Synthesis: Prospects in Visible Light Photocatalysis. *Science* **2014**, *343*, 1239176.

(14) Yoon, T. P.; Ischay, M. A.; Du, J. Visible Light Photocatalysis As a Greener Approach to Photochemical Synthesis. *Nat. Chem.* **2010**, *2*, 527−532.

(15) Xie, J.; Jin, H. M.; Hashmi, A. S. K. The Recent Achievements of Redox-Neutral Radical C−C Cross-Coupling Enabled by Visible Light. *Chem. Soc. Rev.* **2017**, *46*, 5193−5203.

(16) Kärkäs, M. D. Photochemical Generation of Nitrogen-Centered Amidyl, Hydrazonyl, and Imidyl Radicals: Methodology Developments and Catalytic Applications. *ACS Catal.* **2017**, *7*, 4999−5022.

(17) Si, C.; Ma, P. T.; Han, Q. X.; Jiao, J. C.; Du, W.; Wu, J. P.; Li, M. X.; Niu, J. Y. A Polyoxometalate-Based Inorganic Porous Material with Both Proton and Electron Conductivity by Light Actuation: Photocatalysis for Baeyer-Villiger Oxidation and Cr(VI) Reduction. *Inorg. Chem.* **2021**, *60*, 682−691.

(18) Lin, J.; Li, N.; Yang, S.; Jia, M.; Liu, J.; Li, X. M.; An, L.; Tian, Q.; Dong, L. Z.; Lan, Y. Q. Self-Assembly of Giant Mo_{240} Hollow Opening Dodecahedra. *J. Am. Chem. Soc.* **2020**, *142*, 13982−13988.

(19) Li, J.; Chang, B. W.; Zhao, H. Y.; Meng, Q. X.; Li, M. X.; Han, Q. X. Visible-Light-Responsive Polyoxometalate-Based Metal-Organic Framework for Highly Efficient Photocatalytic Oxidative Coupling of Amines. *J. Mater. Sci.* **2021**, *56*, 6676−6688.

(20) Suzuki, K.; Jeong, J.; Yamaguchi, K.; Mizuno, N. Visible-Light-Responsive Multielectron Redox Catalysis of Lacunary Polyoxometalates Induced by Substrate Coordination to Their Lacuna. *Chem. - Asian J.* **2015**, *10*, 144−148.

(21) Sartorel, A.; Bonchio, M.; Campagna, S.; Scandola, F. Tetrametallic Molecular Catalysts for Photochemical Water Oxidation. *Chem. Soc. Rev.* **2013**, *42*, 2262−2280.

(22) Zheng, S. T.; Yang, G. Y. Recent Advances in Paramagnetic-TM Substituted Polyoxometalates (TM = Mn, Fe, Co, Ni, Cu). *Chem. Soc. Rev.* **2012**, *41*, 7623−7646.

(23) Liu, C. S.; Li, J. J.; Pang, H. Metal-Organic Framework-Based Materials as an Emerging Platform for Advanced Electrochemical Sensing. *Coord. Chem. Rev.* **2020**, *410*, 213222.

(24) Li, H. Y.; Zhao, S. N.; Zang, S. Q.; Li, J. Functional Metal-organic Frameworks as Effective Sensors of Gases and Volatile Compounds. *Chem. Soc. Rev.* **2020**, *49*, 6364−6401.
(25) Xu, M. M.; Chen, Q.; Xie, L. H.; Li, J. R. Exchange Reactions in Metal-Organic Frameworks: New Advances. *Coord. Chem. Rev.* **2020**, *421*, 213421.
(26) Li, H.; Yao, S.; Wu, H. L.; Qu, J. Y.; Zhang, Z. M.; Lu, T. B.; Lin, W. B.; Wang, E. B. Charge-Regulated Sequential Adsorption of Anionic Catalysts and Cationic Photosensitizers into Metal-Organic Frameworks Enhances Photocatalytic Proton Reduction. *Appl. Catal., B* **2018**, *224*, 46−52.
(27) Pan, M.; Lin, X. M.; Li, G. B.; Su, C. Y. Progress in the Study of Metal-Organic Materials Applying Naphthalene Diimide (NDI) Ligands. *Coord. Chem. Rev.* **2011**, *255*, 1921−1936.
(28) He, J. C.; Li, J.; Han, Q. X.; Si, C.; Niu, G. Q.; Li, M. X.; Wang, J. P.; Niu, J. Y. Photoactive Metal-Organic Framework for the Reduction of Aryl Halides by the Synergistic Effect of Consecutive Photoinduced Electron-Transfer and Hydrogen-Atom-Transfer Processes. *ACS Appl. Mater. Interfaces* **2020**, *12*, 2199−2206.
(29) Zeman, C. J., IV; Kim, S.; Zhang, F.; Schanze, K. S. Direct Observation of the Reduction of Aryl Halides by a Photoexcited Perylene Diimide Radical Anion. *J. Am. Chem. Soc.* **2020**, *142*, 2204−2207.
(30) Li, J.; He, J. C.; Si, C.; Li, M. X.; Han, Q. X.; Wang, Z. L.; Zhao, J. W. Special-Selective C−H Oxidation of Toluene to Benzaldehyde by a Hybrid Polyoxometalate Photocatalyst Including a Rare $[P_6W_{48}Fe_6O_{180}]^{30-}$ Anion. *J. Catal.* **2020**, *392*, 244−253.
(31) He, J. C.; Han, Q. X.; Li, J.; Shi, Z. L.; Shi, X. Y.; Niu, J. Y. Ternary Supramolecular System for Photocatalytic Oxidation with Air by Consecutive Photo-Induced Electron Transfer Processes. *J. Catal.* **2019**, *376*, 161−167.
(32) Spek, A. L. Single-Crystal Structure Validation with the Program PLATON. *J. Appl. Crystallogr.* **2003**, *36*, 7−13.
(33) Leong, C. F.; Chan, B.; Faust, T. B.; D'Alessandro, D. M. Controlling Charge Separation in a Novel Donor-Acceptor Metal-Organic Framework *via* Redox Modulation. *Chem. Sci.* **2014**, *5*, 4724−4728.
(34) Thouvenot, R.; Fournier, M.; Franck, R.; Rocchiccioli-Deltcheff, C. Vibrational Investigations of Polyoxometalates. 3. Isomerism in Molybdenum(VI) and Tungsten(VI) Compounds Related to the Keggin Structure. *Inorg. Chem.* **1984**, *23*, 598−605.
(35) Wang, D.; Liu, L. L.; Jiang, J.; Chen, L. J.; Zhao, J. W. Polyoxometalate-Based Composite Materials in Electrochemistry: State-of-the-Art Progress and Future Outlook. *Nanoscale* **2020**, *12*, 5705−5718.
(36) Jiang, W.; Liu, X. M.; Liu, J.; Shi, J.; Cao, J. P.; Luo, X. M.; You, W. S.; Xu, Y. A Huge Novel Polyoxometalate-Based Cluster $Fe_{10}P_4W_{32}$ Exhibiting Prominent Electrocatalytic Activity for the Oxygen Evolution Reaction and Third-Order NLO Properties. *Chem. Commun.* **2019**, *55*, 9299−9302.
(37) Xu, L.; Zhang, H.; Wang, E.; Kurth, D. G.; Li, Z. Photoluminescent Multilayer Films Based on Polyoxometalates. *J. Mater. Chem.* **2002**, *12*, 654−657.
(38) Lin, X. Q.; Li, X. Z.; Li, F.; Fang, Y. Y.; Tian, M.; An, X. C.; Fu, Y.; Jin, J.; Ma, J. T. Precious-Metal-Free Co-Fe-O_x Coupled Nitrogenenriched Porous Carbon Nanosheets Derived from Schiff-Base Porous Polymers as Superior Electrocatalysts for the Oxygen Evolution Reaction. *J. Mater. Chem. A* **2016**, *4*, 6505−6512.
(39) Gao, Z. G.; Jia, Z. R.; Wang, K. K.; Liu, X. H.; Bi, L.; Wu, G. L. Simultaneous Enhancement of Recoverable Energy Density and Efficiency of Lead-Free Relaxor-Ferroelectric BNT-Based Ceramics. *Chem. Eng. J.* **2020**, *402*, 125951.
(40) Zheng, S. T.; Zhang, J.; Li, X. X.; Fang, W. H.; Yang, G. Y. Cubic Polyoxometalate-Organic Molecular Cage. *J. Am. Chem. Soc.* **2010**, *132*, 15102−15103.
(41) Zhang, Z.; Wang, Y. L.; Li, H. L.; Sun, K. N.; Yang, G. Y. Syntheses, Structures and Properties of Three Organic-Inorganic Hybrid Polyoxotungstates Constructed from $\{Ni_6PW_9\}$ Building Blocks: from Isolated Clusters to 2-D Layers. *CrystEngComm* **2019**, *21*, 2641−2647.
(42) Wang, X. Q.; Liu, S. X.; Liu, Y. W.; He, D. F.; Li, N.; Miao, J.; Ji, Y. J.; Yang, G. Y. Planar $\{Ni_6\}$ Cluster-Containing Polyoxometalate-Based Inorganic-Organic Hybrid Compound and Its Extended Structure. *Inorg. Chem.* **2014**, *53*, 13130−13135.
(43) Jiang, L.; Choi, H. J.; Feng, X. L.; Lu, T. B.; Long, J. R. Syntheses, Structures, and Magnetic Properties of the Face-Centered Cubic Clusters $[Tp_8(H_2O)_{12}M_6Fe_8(CN)_{24}]^{4+}$ (M = Co, Ni). *Inorg. Chem.* **2007**, *46*, 2181−2186.
(44) Han, L.; Qin, L.; Xu, L.; Zhou, Y.; Sun, J.; Zou, X. A Novel PhotoChromic Calcium-Based Metal-Organic Framework Derived from a Naphthalene Niimide Chromophore. *Chem. Commun.* **2013**, *49*, 406−408.
(45) Wang, X. K.; Liu, J.; Zhang, L.; Dong, L. Z.; Li, S. L.; Kan, Y. H.; Li, D. S.; Lan, Y. Q. Monometallic Catalytic Models Hosted in Stable Metal-Organic Frameworks for Tunable CO_2 Photoreduction. *ACS Catal.* **2019**, *9*, 1726−1732.
(46) Leow, D. Phenazinium Salt-Catalyzed Aerobic Oxidative Amidation of Aromatic Aldehydes. *Org. Lett.* **2014**, *16*, 5812−5815.
(47) Liu, X. Y.; Jensen, K. F. Direct Oxidative Amidation of Aromatic Aldehydes Using Aqueous Hydrogen Peroxide in Continuous Flow Microreactor Systems. *Green Chem.* **2012**, *14*, 1471−1474.
(48) Hsu, Y. C.; Wang, V. C. C.; Au-Yeung, K. C.; Tsai, C. Y.; Chang, C. C.; Lin, B. C.; Chan, Y. T.; Hsu, C. P.; Yap, G. P. A.; Jurca, T.; Ong, T. G. One-Pot Tandem Photoredox and Cross-Coupling Catalysis with a Single Palladium Carbodicarbene Complex. *Angew. Chem., Int. Ed.* **2018**, *57*, 4622−4626.

https://doi.org/10.1021/acs.inorgchem.1c01311
Inorg. Chem. 2021, 60, 10022−10029